ACS OMEGA

http://pubs.acs.org/journal/acsodf

Article

Understanding the Mechanism of Cs Accumulation on Stainless Steel Suspended in Nuclear High-Level Liquid Waste

Kankan Patra,* Arijit Sengupta, Vinit Kumar Mittal, Santanu Bera,* Ashok Kumar Sahu, and Trichur Pisharath Valsala

Cite This: *ACS Omega* 2022, 7, 34190−34199

Read Online

ACCESS | Metrics & More | Article Recommendations

ABSTRACT: In a nuclear facility, the surface of stainless steels (SS) was found to be contaminated during the processing of radioactive liquid waste. Their safe and secure disposal is highly challenging to the nuclear industry. If the fundamental property of steel corrosion could be evaluated, successful decontamination and effective decommissioning strategies could be planned. Although individual radionuclide contamination behavior on SS metal was studied, till date, SS contamination behavior under the exposure of high-level liquid waste (HLLW) was unexplored. In view of this, investigations were carried out to understand the nature of contamination in SS 304L alloy under the exposure of simulated HLLW (SHLLW). For understanding of radionuclide adsorption behavior on structural materials, scanning electron microscopy/energy dispersive X-ray spectroscopy and X-ray photoelectron spectroscopy have been utilized for SS 304L. The solutions were analyzed using inductively coupled plasma optical emission spectroscopy to calculate the changes in the elemental composition of the solution and corrosion behavior of SS. The passivation of SS coupons was observed in the presence of HNO_3 due to enrichment of Cr at the surface. The deposition of Cs and Mo was noticed, while SS coupons were exposed to SHLLW. At 3 M HNO_3 and room temperature, the SS surface is mildly passivated by Cr enrichment by formation of a Cr oxide layer on the SS surface. However, the passive layer was not thick enough to attenuate the signal from the substrate below the passivated layer. Hence, Fe^0 and Cr^0 were also found along with Cr^{3+} and Fe^{3+} (in small quantity). When temperature was elevated to 70 °C, the SS surface was completely covered with the Cr oxide layer, and hence no Cr^0 signal was observed. The small signal of Fe^0 indicated that the signal from the substrate surface is present below the passive layer. During the passivation process, Cr diffused toward the passive layer, thereby producing a Cr-depleted layer below the passive layer (Cr^0 signal was not seen). In the case of SHLLW at 70 °C, the surface was fully covered by Cr^{3+}, Mo^{6+}, and Cs^+. Fe and Ni were not observed at all. This finding will help to design an effective corrosion inhibitor and suitable decontamination agent. In addition to that, this information was found to be useful in designing high-performance novel and modern age reactor materials with improved characteristics.

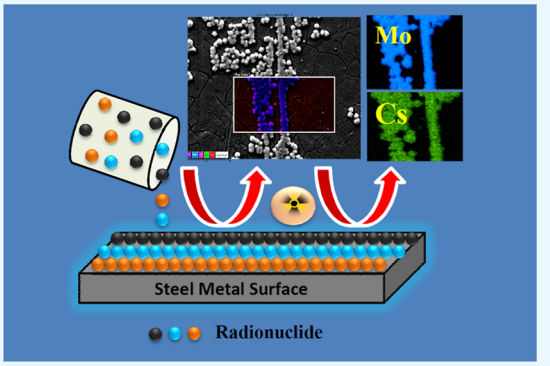

INTRODUCTION

A low carbon-based power production is a worldwide priority compared to the utilization of fossil fuel power. Though nuclear energy is one of the viable resources, the spent fuel generated during nuclear reactor operation contains large amounts of hazardous solid radioactive waste, which is of high potential risk to the environment and mankind unless properly managed.[1,2] Significant volumes of radioactive waste arise due to accumulation of radionuclides from the aqueous solution onto the nuclear plant materials surface.[3] Owing to the extensive use of stainless steels such as SS 304L as storage and structural materials[4] at nuclear facilities, these alloys become a main source of solid radioactive waste. Globally, the total volume of radioactive SS is not estimated, but definitely, they make a considerable waste volume.[5] In the nuclear industry, the selection of SS is due to combination of two advantages; first one is a high radiation resistance capacity and second one is an excellent corrosion inhibition property, as it can easily form a rapid passive Cr oxide layer.[6] During the accumulation process, the deposited radionuclides were found to adsorb within the passive layer.[7] After getting in contact with the aqueous medium, the passive oxide becomes charged and start to interact with dissolved ions electrostatically.[8] The surface complexation process for radioactive metal ions transport[9] has been used to illustrate sorption characteristics.[10,11] However, in

Received: June 6, 2022
Accepted: August 19, 2022
Published: September 14, 2022

recent times, studies on the sorption process were found to be more complex in nature, where complete characterization is not achievable by using charge principles alone.[12] The structure, elemental composition, and thickness of the surface oxide layer may change with the variation in the composition and potential of the passivating medium;[13] therefore, the derived sorbent characteristics are likely to reflect both steel composition, as well as environment chemistry. Hence, the "plate-out" process and corrosion behavior of metal need to be critically investigated under the conditions of a nuclear facility.

Research has been carried out to explore the mechanism of binding radioactive element to SS surfaces and find out an environmentally friendly decontamination process that most effectively eliminates the hazardous contaminant.[14−16] Extensive efforts have been made to manage structural materials, that is, SS from nuclear facilities. Research has been focused predominantly on understanding the fission product and transuranic binding mechanisms on the SS surface.[16−19] However, most of the studies are carried out with a solution medium based on contamination processes with SS for short periods of exposure time (i.e., hours) under room temperature and a weakly acidic condition.[16] It has been observed that there are several possible contamination mechanisms that are operating such as "loose "or "fixed."[20] However, the nature of SS contamination under the exposure of HLLW is really missing so far, which is indeed essential for the execution of effective decontamination. To the best of our knowledge, this is the first attempt where all the concerned elements in nuclear liquid waste are allowed to interact with SS under 70 °C for 120 days so that we can present a complete picture of contamination behavior and corrosion impact on SS.

In view of this, efforts were put to evaluate the extent as well as nature of nuclear waste contamination on SS 304L surfaces at 70 °C and room temperature for a duration of 120 days. The prime objective of long exposure is to determine the impact of long-term nuclear waste corrosion on metal surfaces under similar conditions at nuclear facilities. Initially SS coupons were exposed to HNO_3, SHLLW, and in combination of both at room temperature and at 70 °C. The exposed coupons surfaces were characterized by the XPS technique for a fundamental understanding of the corrosion nature and deciding the method for chemical decontamination. Evaluation of the surface morphology and elemental composition changes of the corroded metal surface was carried out by SEM/EDX and X-ray elemental mapping. The exposed solutions were characterized with the ICP-OES technique to understand the changes in the metal ion concentration at various times. The main aim of the present investigation is to provide insights into the corrosion behavior and mechanism of interaction of the deposited element on SS 304L, which would be useful in designing appropriate decontamination strategies for post-operational effective decontamination and safe decommissioning of nuclear facilities.

EXPERIMENT

Materials and Methods. SS 304L-type materials were used for the present study. Prior to starting the experiments, materials were ground using SiC paper (from P120 to P2500) and thoroughly polished (first 6 μm, then using 1 μm diamond paste). SHLLW was prepared with HLLW composition, as described in Table 1. SS coupons were placed completely in a container containing SHLLW solutions of 3 M HNO_3 (100 mL). Table 2 represents the details of sample (SS 304L) preparation and nomenclature. Samples were prepared using 3 M SHLLW solutions at room temperature and with solutions containing just 3 M HNO_3 with SS coupons at 70 °C for 120 days. All experiments were carried out in triplicate. After the allocated time, the coupons were removed carefully from the solution and ready for surface characterization. The solutions were analyzed with ICP-OES for evaluation of the elemental composition of the solution with respect to different exposure times. After removal of the SS coupons from the solution, the surface of the coupons was rinsed thoroughly using deionized water. This initial washing was carried out to avoid post-immersion contamination and eliminate effectively any acidic solution from the SS coupon. During the washing of coupons, if any contaminant was eliminated, then it was considered that it has been bound weakly, so it was not relevant to this

Table 1. Composition of Simulated HLLW

s. no	property	quantity
01	molarity acidic (M)	3
02	alpha activity (Ci/L)	1.86
03	beta activity (Ci/L)	45−50
04	isotopic composition	
	Cs-137 (Ci/L)	14
	Cs-134 (mCi/L)	47.0
	Eu-154 (mCi/L)	138.6
	Eu-152 (mCi/L)	12.2
	Sb-125 (mCi/L)	21.6
	Ce-144 (mCi/L)	16.8
	Ru-106 (mCi/L)	14.8
	Zr-95 (mCi/L)	4.7
	Sr90−Y90 (Ci/L)	34
	Am241 (Ci/L)	0.85
	Pu 239 (Ci/L)	1.0
05	elemental composition (mg/L)	
	Na	8.20
	U	3.32
	Fe	1.04
	Mn	0.78
	Cr	0.25
	Ni	0.13
	Ce	0.74
	La	0.45
	Nd	1.38
	Sm	0.28
	Pr	0.18
	Eu	0.005
	Y	0.12
	Ru	0.62
	Pd	0.31
	Sr	0.22
	Ba	0.51
	Mo	0.51
	Zr	0.01
	Al	0.04

Table 2. Details of Sample (SS 304L) Preparation and Nomenclature

s no	solution nature	temperature
sample 1 (SW70)	S HLLW	70 °C
sample 2 (SWRT)	S HLLW	room temp
sample 3 (HN70)	3 M HNO_3	70 °C
sample 4 (HNRT)	3 M HNO_3	room temp

https://doi.org/10.1021/acsomega.2c03535
ACS Omega 2022, 7, 34190−34199

experiment. The coupons were then allowed to air-dry at room temperature for 30 min before weighing.

Scanning Electron Microscopy/Energy Dispersive X-ray Spectroscopy (SEM/EDX). Microstructural characterization of the exposed metal surface was carried out using FEG-SEM (Model AURIGA, ZEISS) equipped with EDS (Oxford) to study the adsorption and distribution of radionuclides on the surface of the material. A representative sample, which was exposed to SHLLW for 120 days at 70 °C, was coated with a thin layer of gold to prevent charging. X-ray elemental mapping was also performed.

X-ray Photoelectron Spectroscopy. The deposited chemical compositions of the oxide layer formed on the SS surface and the chemical environment were explored using XPS by using a VG ESCALAB MK200X system using Al kα as the X-ray source. The system was calibrated with a Au $4f_{7/2}$ line at 84.0 eV with 1.6 eV FWHM. The C 1s peak of the contaminant was taken at 285.0 eV for charge correction.

Solution Analysis. Different metal ions uptake from SHLLW was studied at different time intervals using ICP-OES (SPECTRO ARCOS, Germany). Triplicate measurements were performed to report each data.

RESULTS AND DISCUSSION

Surface Microstructure and Microanalysis. To understand the details of the passivated layer on SS 304L and mechanism of Cs and Mo adsorption with SHLLW at room temp (RT) and 70 °C, the samples were studied by SEM and EDX. SEM images (Figure 1a,b) show the surface morphology after immersion in the concentrated 3 M HNO_3 contaminating SHLLW at 70 °C for 120 days. It reveals the formation of crystallites nonuniformly distributed all over the surface. Formations of two layers are identified, as marked by Figure 1a,b. It is assumed that the inner layer (b) is grown on the SS substrate, and the partially formed outer layer (a) is formed due to nucleation and growth on the inner layer by the hydrothermal process. EDS recorded on the inner layer confirmed that the passivation of SS has taken place as there was enrichment of chromium on the surface, which was further confirmed by XPS. Cs, Fe, Mo, and O were observed to be present in the second layer. X-ray maps of various elements on a face consisting of both the adsorbed and passivated surface further complimented our findings. We present our finding in the following subsection.

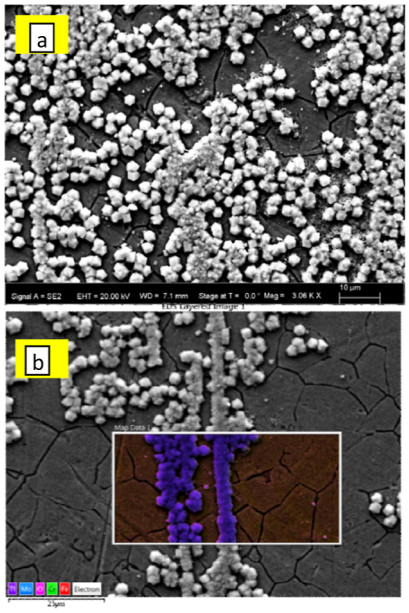

Figure 1. Micrograph of the sample (SS 304L exposed to SHLLW at 70 °C for 120 days); (a) outer layer composed of crystallites and (b) inner layer without any crystallites.

From Figure 1, it was observed that the average size of the crystallites deposited was ~3 μm. It was scattered inhomogeneously all over the surface. The inner layer is the Cr_2O_3 layer, and the outer layer is partially covered by the formation of crystallites containing Cs^+ and MoO_4^{2-} ions. It is clear that the size of the crystallites is limited by a certain critical size, and the inner layer is covered by the growth and nucleation of new crystallites. For an easy discussion, the two layers are mentioned. It appears that with prolonged exposure to the SHLLW, the inner layer will be covered completely depending on the availability of the constituent ions in the solution. Figure 1a represents the inhomogeneous distribution of metal ions all over the surface. Figure 1b indicates the partially formed outer layer by Cs^+ and MoO_4^{2-} ions. The micrograph reveals the second formation of the passivated layer on the surface due to the interaction of elements present in SHLLW. It is essential to evaluate the chemical composition of the deposited layer. X-ray elemental mapping of the surface layer was carried out. Figure 2a clearly shows the electron image of the passivated layer on steel alloy. Spectrum 1 (Figure 2b) represents the base metal characteristics under an exposed condition at 70 °C for 120 days of suspension in SHLLW. Spectrum 1 indicates the Fe-rich surface area (around 70%) along with Cr (around 20%) layer formation on the exposed surface. From spectrum 2 (Figure 2c), it was observed that Cs (13 wt %) and Mo (30 wt %) along with oxygen (around 35%) were found to be present on the passivated surface. Therefore, after the interaction with SHLLW, Cs- and Mo-enriched passivated layer formation took place on the metal surface, which was further explored by XPS and ICP-OES analyses. From Figure 3, it is clear that the base metal is Cr enriched. X-ray elemental mapping revealed the significant presence of Mo and Cs in the passivated layer (Figure 3). The dissolution of Fe and Ni took place in the presence of 3 M HNO_3 at 70 °C, resulting in the formation of a Cr-enriched passivated layer. Among several elements in SHLLW (Table 1), only Cs and Mo were deposited. At 70 °C, under the solution phase, the Cr elemental state is relatively more stable than Fe and Ni,[21] resulting in higher dissolution of Fe and Ni than Cr, as confirmed by ICP-OES analysis. Cs and Mo were found to be deposited from SHLLW on the SS surface. It may be proposed that from the SS surface, Fe and Ni were removed as cations, leading to a negative surface charge on the SS surface. This negative charge surface showed a strong affinity for H^+, Cs^+, or ($2Cs^+$–MoO_4^{2-}), resulting in deposition of Cs and Mo, as indicated by EDX analysis and confirmed by XPS and ICP-OES solution analysis.

For better understanding of the exposed SS (sample SW70) surface, X-ray elemental mapping was carried out. From Figure 3, it is clear that the inner layer is Cr enriched. X-ray elemental mapping revealed that the second layer elemental composition enriched with Mo and Cs (Figure 3). The dissolution of Fe and Ni took place in the presence of 3 M HNO_3 at 70 °C, which was not redeposited on the SS surface, as confirmed by X-ray elemental mapping and ICP-OES solution analysis

https://doi.org/10.1021/acsomega.2c03535
ACS Omega 2022, 7, 34190−34199

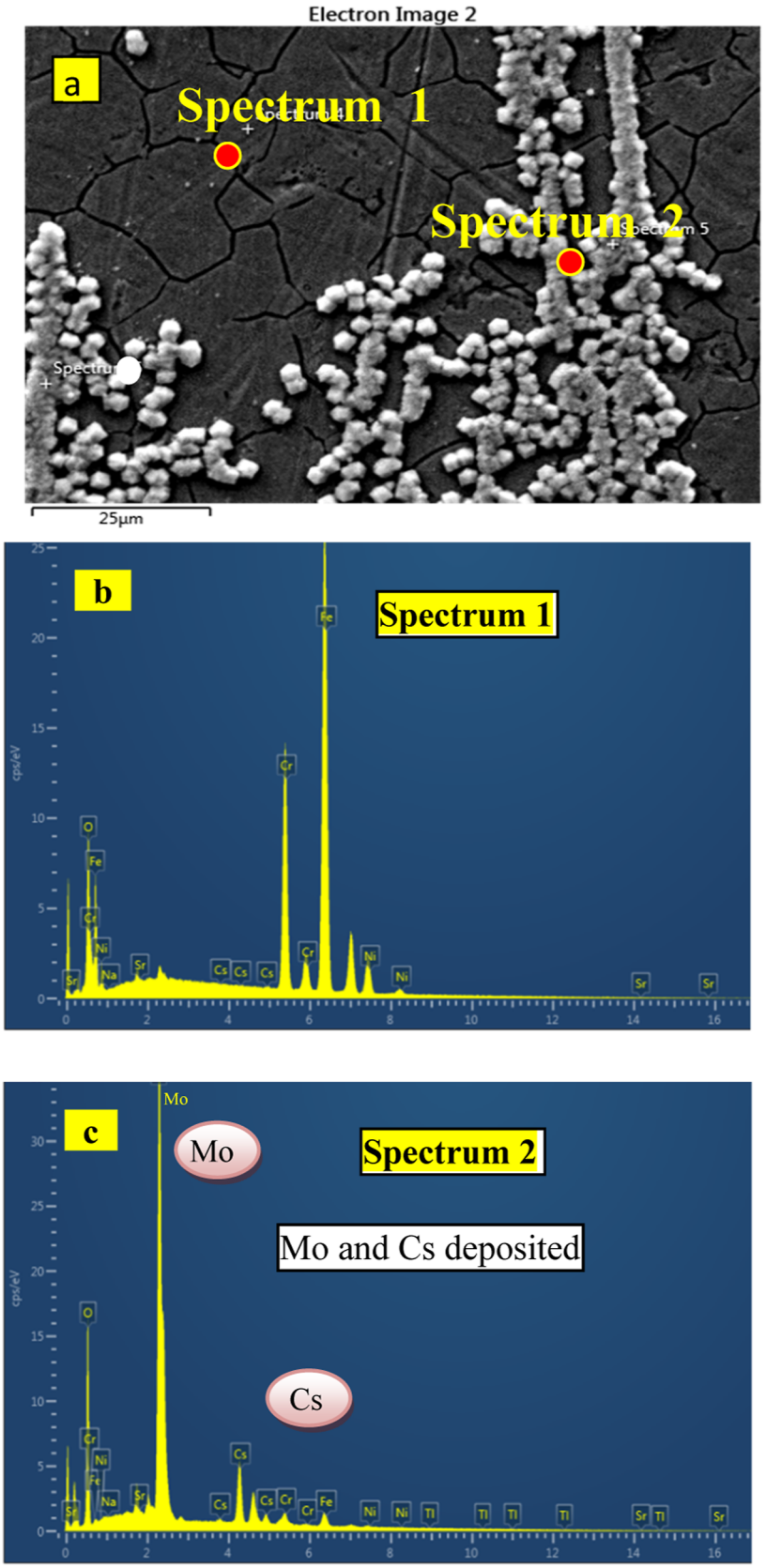

Figure 2. (a) Electron image of the passivated layer on the steel alloy, (b) spectrum of the passivated layer without the crystallite (spectrum 1), and (c) spectrum of the passive layer with crystallites (spectrum 2).

discussed later. Among all the elements present in SHLLW (Table 1), only Cs and Mo were deposited preferentially. Therefore, it was confirmed that Cs and Mo both play a key role in elemental deposition.

https://doi.org/10.1021/acsomega.2c03535
ACS Omega 2022, 7, 34190−34199

Figure 3. X-ray elemental mapping of the passivated layer with a crystallite on the metal surface.

Under an acidic aqueous condition, preferential dissolution of Fe and Ni leads to the formation of a Cr_2O_3 protective surface film. However, when the acidity of the solution was high (3 M HNO_3), the oxidizing power was good enough to convert insoluble Cr(III) to soluble Cr(VI) species.

The consequent removal of Cr from the metal surface weakens the protective film, later resulting in corrosion of the metal.[22] Under the strong oxidizing environment, failure of this passive layer is termed transpassive behavior, which leads to the initiation of corrosion phenomena at Cr depletion sites.[23,24] In our studied system, under 3 M HNO_3, base metal dissolution was observed, that is, mass transfer from metal to solution and adsorption of contamination from acidic medium took place (Figures 2 and 3). After exposure to an acidic solution, the passive film layer was observed to thicken gradually, which is confirmed in Figure 3, as a persistent oxygen signal was observed from X-ray elemental mapping. The gradual growth of the thicker films is correlated with a

https://doi.org/10.1021/acsomega.2c03535
ACS Omega 2022, 7, 34190−34199

bilayer model for the metal passive layer structure. The inner passive layer is composed of Fe oxide and a partially formed outer layer enriched with Cr_2O_3.[21,25] The partially formed outer layer has shown stability in a neutral and slightly acidic medium.[26] In the presence of 3 M HNO_3, when the passive film of Fe oxide starts to interact, Fe oxide leached into the aqueous phase as Fe can easily dissolve in a highly acidic region, resulting in a Cr-enriched passive layer. Table 3 clearly

Table 3. Comparison of the Elemental Composition of the Passive Layer without the Crystallite and Passivated Layer with the Crystallite of SS

element	line type	spectrum 1 (wt %)	spectrum 2 (wt %)	standard label
O	K series	8.95	29.16	SiO_2
Na	K series	0.15	0.00	Albite
Cr	K series	21.96	1.16	Cr
Fe	K series	61.21	1.69	Fe
Ni	K series	7.49	0.13	Ni
Cs	L series	0.23	13.24	Cs (v)
Mo	L series	0.00	31.28	Mo

indicates the composition of spectrum 1 and spectrum 2, and it reveals that the crystallite on the passive layer (spectrum 2) contains Cs (wt 13.24%) and Mo (wt 31.28%), whereas, on the clear passive layer (spectrum 1), no such Cs and Mo were observed. In addition, X-ray elemental mapping (Figure 3) clearly indicates the deposition of Cs and Mo.

Surface Chemical Analysis. Figure 4 shows the XPS results recorded from 3 M HNO_3-exposed coupons at RT and

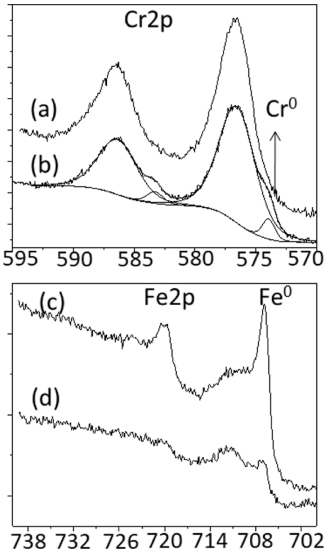

Figure 4. XPS spectra of Cr 2p from (a) HN70, (b) HNRT; the arrow indicates the presence of Cr^0 in the spectrum, (c) Fe 2p from HNRT, (d) Fe 2p from HN70.

70 °C. The room-temperature-exposed coupon (sample HNRT) showed a mild passivation due to the enrichment of Cr and formation of a Cr oxide layer on the SS surface. However, the passive layer was not thick enough; as a result, elemental Fe^0 (Figure 4b) and Cr^0 signals were observed from the base substrate. While in the case of the coupon exposed to 70 °C and HNO_3 (sample HN70), the passive layer (Cr enrichment) was more prominent, and Fe^0 and Cr^0 peaks were not observed.

The surface chemical analysis of SS coupons exposed to SHLLW at RT and 70 °C is shown in Figure 5. In the case of

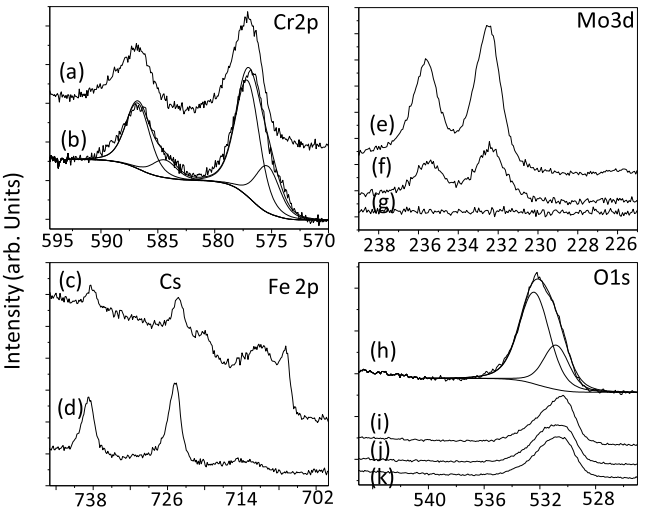

Figure 5. (a) Cr 2p from SW70, (b) Cr 2p from SWRT. (c) Fe 2p from SWRT, (d) Fe 2p from SW70; presence of Cs was detected on the surface. (e) Mo 3d from SW70, (f) Mo 3d from SWRT, (g) Mo 3d from HN70. (h) O 1s from SW70, (i) O 1s from SWRT, (j) O 1s from HNRT, and (k) O 1s from HN70.

the SHLLW-exposed coupon at room temperature (sample SWRT), the surface was seen to contain Mo and Cs. Mo is present in +6 states, and Cs is in the +1 state. In Figure 6, the

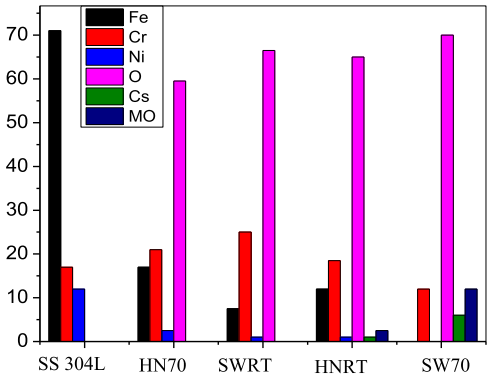

Figure 6. Bar chart of the atomic concentration of the elements obtained from XPS analysis. SS 304L: standard SS 304L, HNRT: HN70, SWRT, and SW70.

concentration of different elements on the surface is shown by the bar chart. In the sample SWRT, the concentration of Mo is more compared to Cs, probably due to the availability of Mo is more than Cs in the SHLLW solution. As expected, the Cr^0 and Fe^0 signals from the substrate was observed, as shown in Figure 5b,c. In the case of SHLLW at 70 °C (sample SW70), the surface is fully covered by Cr^{3+} and Mo^{6+} and Cs^+. Fe and Ni were not observed at all. Even though HLLW contains more than 25 elements, only Cs and Mo were getting deposited. The relative concentration of metals with oxygen is shown in Figure 6. In fact, O concentrations were very high in the range of 60−70 at. %. High O concentrations visually reduced the sharp variation in the concentrations of other

https://doi.org/10.1021/acsomega.2c03535
ACS Omega 2022, 7, 34190−34199

elements, especially Cs and Mo. The oxygen concentrations for the HNO_3 medium at room temperature and 70 °C is around 60−65 at. %, and that for SHLLW case, it was 65−70 at. %.

Mechanism of Cs and Mo Adsorption. There are two different processes that took place for the growth of the layer on the SS surface. The inner layer composed of Cr_2O_3 is formed due to preferential dissolution of Fe and Ni, leaving the surface Cr enriched. Oxygen carrying species react with the Cr layer to form the Cr_2O_3 passive layer in the acid medium. The second layer is formed by nucleation and subsequent growth of the crystallites containing Mo and Cs by the hydrothermal process.

The solution pH is important for the initiation of the adsorption process. The zeta potential of the Cr_2O_3 layer is positive in the acidic condition.[27] High acid molarities lead to the protonation of the surface and activate it for the nucleation of the crystallites. Adsorption of MoO_4^{2-} is assumed to be chemisorption due to the following reactions

$$Cr - OH - Cr + MoO_4^{2-} + 2H + \rightarrow Cr_2MoO_4^{2-} + H_2O \rightarrow +Cs \rightarrow Cr - Mo - O - Cs \text{ inner sphere complexes}$$

The nucleation involving both Cs and Mo further grew through the hydrothermal process, leading to the formation of the crystallites. It is observed that the crystallites are grown to a certain critical size (3 μm) and grow laterally and thereby increasing the surface coverage of the crystallites. The mechanism is shown schematically in Figure 10.

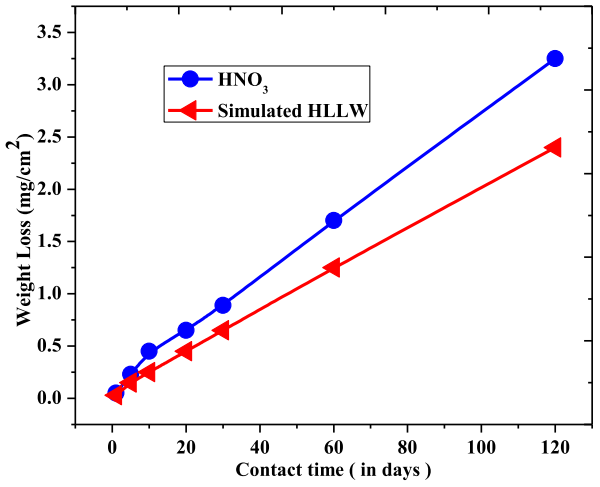

Figure 7. Corrosion rate of polished SS 304L coupons for 120 days exposure in contact with 3 M nitric acid (100 mL) and 3 M SHLLW at 70 °C.

Recently, the corrosion effect of Cs and Sr (nuclear fission product) on AISI Type SS 304L was studied under an acidic condition (HNO_3).[28] Experimental results revealed that under an acidic condition, the SS surface was passivated with Cr_2O_3, which is very similar to our experimental results. Cs and Sr were deposited on the Cr_2O_3 passive layer.[28] Similarly, the effect of long-term uranium (U) corrosion on SS 304L was studied under an acidic condition.[29] Uranium was deposited all over the SS surface. The Uranium uptake on SS reached equilibrium after 14 days. From Raman microscopy, X-ray absorption spectroscopy, and synchrotron microfocus X-ray

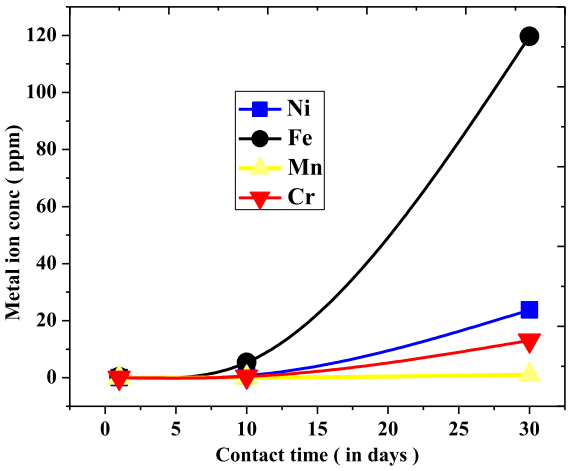

Figure 8. ICP-OES measurements of the Cr, Fe, Mn, and Ni solution concentration variation against the exposure length of SS 304L coupons to solutions of 3 M HNO_3 (100 mL) at 70 °C.

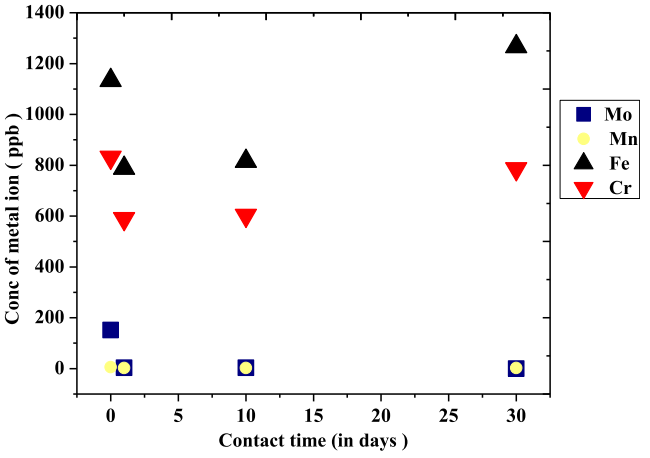

Figure 9. ICP-OES measurements of the Mo, Fe, Mn, and Cr solution concentration variation against the exposure length of SS 304L coupons to solutions of 3 M SHLLW (100 mL) at 70 °C.

fluorescence, inhomogeneous localization of the uranium element coupled with the oxide layer was observed on the SS surface.[29] Corrosion resistance of SS 304L, Inconel 718, and trim chromium was studied under acidic and alkaline electrolytes conditions.[30] The microstructural characterization and potentiodynamic (PD) parameters of these alloys were evaluated. Surface analysis of the corroded alloys after potentiodynamic studies clearly revealed that the intermetallics dominated with iron metal and nickel and copper were found relatively low in the presence of Cl^- solution.[30] Recently, long-term corrosion of multiphase alloy and oxide material were examined under geologic disposal conditions.[31] They confirmed that electrochemical impedance spectroscopy altered the electrical properties of the alloys surfaces and corrosion rates. Those methods gave a quantitative evaluation of corrosion for long-term waste disposal assessments and alternative methods that do not change the alloy surface properties. Very recently, Gattu et al. explored the electrochemical corrosion effects on two multiphase alloys made of SS 304L and different proportions of metallic fuel waste.[32] PD scans and SEM studies were carried out to evaluate the complex corrosion behavior of the alloys, as well as electrochemical responses of the specific phase of the alloys

https://doi.org/10.1021/acsomega.2c03535
ACS Omega 2022, 7, 34190−34199

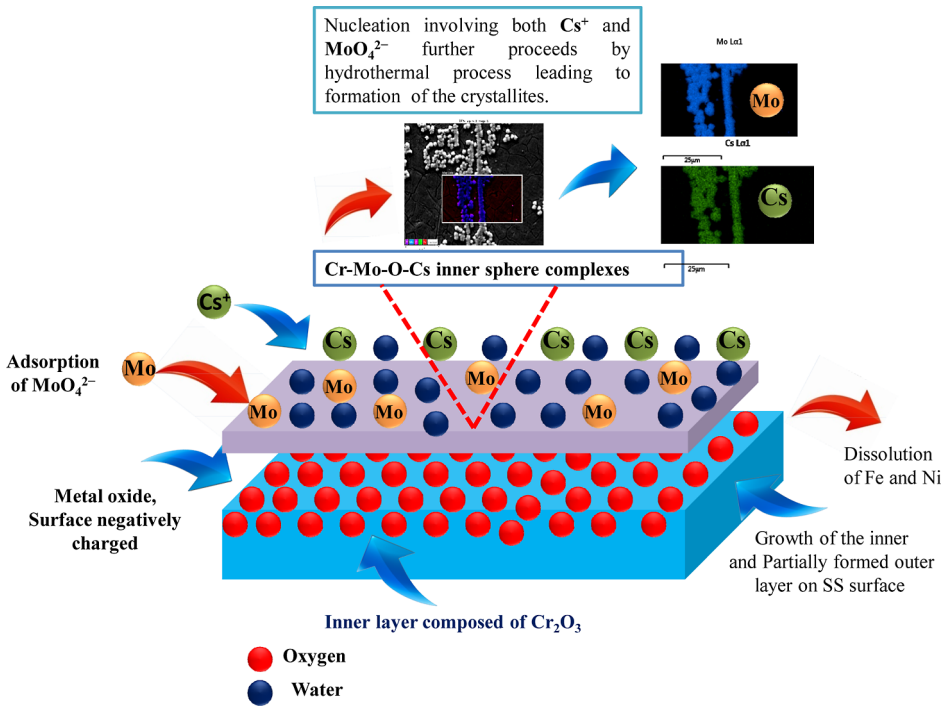

Figure 10. Overall mechanism of nucleation of Cs and Mo containing species on SS and its growth to crystallites.

due to corrosion. From the microstructural characterization of the alloys, ferrite species and intermetallic $FeZr_2$ phases were observed. The PD scan confirmed that the corrosion of the alloys was sensitive to the ferrite composition present in the waste form.

Elucidating Corrosion Behavior through Solution Analysis. SS samples were exposed to 3 M HNO_3 and 3 M SHLLW solutions for 120 days at 70 °C. The weight loss of the SS coupons was measured with respect to different contact times. A linear relationship between the weight loss of coupons and the time of exposure was studied (Figure 7). The weight loss of the SS when exposed to 3 M HNO_3 was found to be comparatively higher than that of 3 M SHLLW (Figure 7). It can be attributed to the deposition of Cs and Mo on the passivated layer under SHLLW contact at 70 °C over a long time period. In the case of pure HNO_3, only corrosion was found to occur, resulting in gradual weight loss. However, in the case of SHLLW, corrosion, as well as elemental deposition, was evidenced from SEM, EDX, and XPS analyses. Hence, the weight loss under SHLLW condition was found to be lower compared to that with the pure HNO_3 medium.

In general, for SS metal, iron and chromium both were found to form the passive film layer to protect the bulk materials from the corrosion effect under an acidic medium.[29,33] Under this condition, the thickness of the passive layer can be around a few nanometers in the presence of sufficient oxygen.[33] Growth of the films directly depends on the diffusion of metal ions to the solution. The solution after exposure of 3 M HNO_3 at 70 °C for 120 days was analyzed by ICP-OES, indicating the presence of Cr, Fe, Mn, Mo, and Ni. Basically, it was a mass transfer from the solid surface to the solution phase, as depicted in Figure 8. The maximum dissolution took place for Fe, resulting in a Cr-enriched passivated layer.

In the case of SHLLW at 70 °C for 120 days of exposure, the Mo concentration from the solution was observed to decrease drastically (Figure 9), indicating fast Mo uptake on the SS surface, as confirmed by the characteristic XPS peak of Mo. In the case of Fe and Cr, initially, the concentrations were found to decrease; afterward, they started increasing. In the case of Mn, a gradual reduction in the concentration with time was evidenced. The corrosion rate of SS is influenced by the dissolved ions in the solution. (i) The corrosion process is controlled by both anodic (oxidation) and cathodic reactions. In general, the anodic reaction is $Fe \rightarrow Fe^{2+} + 2e^-$ and the cathodic reaction is $2H^+ + 2e^- = H_2$. Hence, the dissolved ions in the solution influence the corrosion rate. In the present case, the SS sample is surrounded by several cations and anions and hence the equilibrium of the redox reaction is changed. (ii) The surface of the SS is gradually covered with the Mo−Cs oxide, which reduced the surface area in contact with the acid, and hence the Fe dissolution is reduced. The concentrations of Cr and Fe in HNO_3 and SHLLW after 30 days are compared (Figures 8 and 9). From Figure 8, the Cr concentration in HNO_3 is around 13 ppm, whereas it is only 0.8 ppm in SHLLW. The Fe/Cr concentration was reduced in SHLLW, indicating that Fe dissolution was reduced in comparison to Cr in the SHLLW. It is assumed that the Cr-enriched layer in spectrum 1 (SW70) gets oxidized in the redox process, resulting in Cr dissolution from the top surface. As Fe resides at the lower part of the Cr-enriched layer, its dissolution is comparatively lower than Cr in SHLLW.

Proposed Corrosion Inhibitor for the Studied System. In the present study, the dissolution of Fe and Ni from the base alloy was observed from ICP-OES analysis, resulting in corrosion of metal started through the transfer of electrons from Fe and Ni to an external electron receiver, hence the release of metal into the solution and degradation of the metal surface.[34] The behavior of any suitable inhibitor strongly depends on the availability of the electrons from donor atoms. If the electron density of the donor atom is high, then the efficiency of the inhibitor increases. In the case of the corrosion

https://doi.org/10.1021/acsomega.2c03535
ACS Omega 2022, 7, 34190−34199

inhibitor, the first step is Schiff base molecule adsorption on the SS surface, requiring an available empty low-level vacant orbital of the metal. The inhibitor must have heteroatoms containing free lone pair electrons, which can easily interact with the metal empty orbital.

To the best of our knowledge, we proposed 2,2′(thiophene-2,5 diylbis (methanylylidene)) bis(*N*-phenylhydrazinecarbothioamide) (SS2)[35] (Figure 11) compound as a suitable

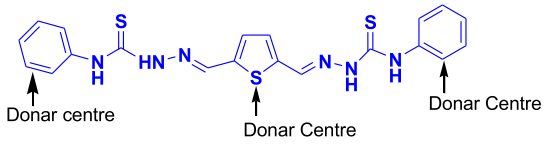

Figure 11. Chemical structure of 2,2′-(thiophene-2,5 diylbis (methanylylidene))bis(*N*-phenyl hydrazine carbothio amide) (SS2).

inhibitor for the present system. It would be the best possible inhibitor for SS corrosion, probably owing to the availability of conjugated π electrons of the phenyl moiety and also heteroatoms contain lone-pair electrons on SS2, which save the steel surface from corrosion. Figure 12 represents the mechanism of protection of the steel surface from corrosion by creating an organic layer on the surface.

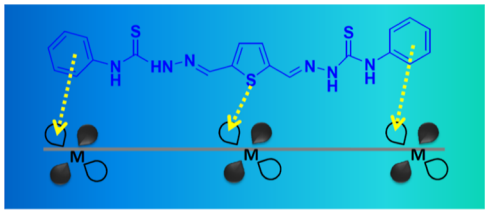

Figure 12. Proposed mechanism of inhibitor interaction.

The performance of the corrosion inhibitor depends on the chemical stability under the working conditions, and here the proposed inhibitor SS2 exhibits stability under a nuclear processing environment, including temperature, an acidic medium, and a radiolytic condition.[35,36] Corrosion inhibitor SS2 can form a strong coordination bond with Cr_2O_3, resulting in the formation of a protective layer over the passive layer. The electron-rich π bond will interact with the vacant orbital of the Cr element, making strong pi-electron and d-electron interactions. As it is anticipated that the inhibitor SS2 makes a strong protective layer by making a strong chemical interaction on the passive oxide layer, hence the proposed inhibitor has significant potential to avoid the unwanted deposition of Cs−Mo−O on the steel surface.

CONCLUSIONS

The impact of corrosion on the accumulation of Cs on SS 304L due to long-term exposure with SHLLW has been investigated. The steel coupons were exposed to 3 M HNO_3 and 3 M SHLLW under room temperature and 70 °C. SEM and EDX analysis indicate the formation of crystallites nonuniformly distributed all over the SS surface. Formation of two layers on SS is identified, the inner layer enriched with Cr is grown on the SS substrate, and the partially formed outer layer composed of Cs and Mo is formed due to nucleation and growth on the inner layer. In addition, X-ray elemental mapping revealed the distribution of Mo and Cs on the SS surface. XPS analysis shows the formation of the Mo−Cs−O-containing phase on the Cr_2O_3 layer on the coupons exposed at 70 °C in SHLLW. The solution analyzed by ICP-OES after exposure of 3 M HNO_3 at 70 °C for 120 days indicates that maximum dissolution took place for Fe, resulting in a Cr-enriched passive layer, which is assumed to be primarily responsible for nucleation of Mo−Cs−O crystallites.

From a mechanistic point of view, there are two different processes that took place for the growth of the inner and partially formed outer layer on the SS surface. The inner layer is composed of Cr_2O_3 due to preferential dissolution of Fe and Ni leaving the Cr-enriched surface. Oxygen-carrying species react with the Cr layer to form a Cr_2O_3 passive layer under an acid medium. The second layer is formed by nucleation and subsequent growth of the crystallites containing Mo and Cs by the hydrothermal process. High acid molarities lead to the protonation of the surface and activate it for the nucleation of the crystallites. Adsorption of MoO_4^{2-} is assumed to be chemisorption due to the formation of Cr−Mo−O−Cs inner-sphere complexes. The nucleation involving both Cs and Mo further grew through the hydrothermal process, leading to the formation of the crystallites. It is observed that the crystallites are grown to a certain critical size (3 μm) and grow laterally. thereby increasing the surface coverage of the Cr-enriched passive layer. Based on the experimental results, we proposed SS2 will be the best suitable inhibitor, which can form a protective layer on the passive layer, resulting in minimization of the deposition of Cs^+ and Mo^{6+} on the SS 304L surface. These experimental results also suggest a new avenue for the effective decontamination method for SS 304L exposed to acidic SHLLW. This work will help in designing and executing management schemes for radioactive solid waste, as well as subsequent decommissioning at nuclear facilities.

AUTHOR INFORMATION

Corresponding Authors

Kankan Patra − *Nuclear Recycle Board, Bhabha Atomic Research Centre, Tarapur 401504, India;* orcid.org/0000-0003-3388-5768; Email: kankan.patra2010@gmail.com

Santanu Bera − *Homi Bhabha National Institute, Mumbai 400 094, India; WSCD, BARC Facilities, Kalpakkam, Tamil Nadu 603 102, India*; Email: bera@igcar.gov.in, berajp@yahoo.com

Authors

Arijit Sengupta − *Radiochemistry Division, Bhabha Atomic Research Centre, Mumbai 400 085, India; Homi Bhabha National Institute, Mumbai 400 094, India*

Vinit Kumar Mittal − *Nuclear Recycle Board, Bhabha Atomic Research Centre, Tarapur 401504, India*

Ashok Kumar Sahu − *Glass & Advanced Materials Division, Bhabha Atomic Research Centre, Mumbai 400085, India*

Trichur Pisharath Valsala − *Nuclear Recycle Board, Bhabha Atomic Research Centre, Tarapur 401504, India*

Complete contact information is available at: https://pubs.acs.org/10.1021/acsomega.2c03535

Notes

The authors declare no competing financial interest.

https://doi.org/10.1021/acsomega.2c03535
ACS Omega 2022, 7, 34190−34199

■ ACKNOWLEDGMENTS

Authors acknowledge U. Dani, G.M., R&WM, BARC (T), Dr. R. Acharya, Head, Actinide Spectroscopy Section, RCD, BARC, Dr. H. Pal, Professor, Homi Bhabha National Institute & Former Associate Director, Chemistry Group, BARC, Mumbai, and Dr. Biswajit Sadhu, Scientific Officer, HPD, BARC, Mumbai.

■ REFERENCES

(1) Rivasseau, C.; Farhi, E.; Atteia, A.; Couté, A.; Gromova, M.; de Gouvion Saint Cyr, D. d. G.; Boisson, A.-M.; Féret, A.-S.; Compagnon, E.; Bligny, R. An extremely radioresistant green eukaryote for radionuclide bio-decontamination in the nuclear industry. *Energy Environ. Sci.* **2013**, *6*, 1230−1239.
(2) Brumfiel, G. Fukushima set for epic clean-up. *Nature* **2011**, *472*, 146−147.
(3) International Atomic Energy Agency. Management of spent fuel from nuclear power reactors. *Proceedings of an International Conference*. STI/PUB/1661; International Atomic Energy Agency: Vienna, 2006.
(4) Shaw, R. D. Corrosion prevention and control at Sellafield nuclear fuel reprocessing plant. *Br. Corros. J.* **1990**, *25*, 97−107.
(5) Nieves, L. A.; Chen, S. Y.; Kohout, E. J.; Nabelssi, B.; Tilbrook, R. W.; Wilson, S. E. Analysis of disposition alternatives for radioactively contaminated scrap metal. *J. Franklin Inst.* **1998**, *335*, 1089−1103.
(6) McGuire, M. F. *Stainless steels for design engineers*; ASM International: Ohio, 2008.
(7) Castellani, R.; Poulesquen, A.; Goettmann, F.; Marchal, P.; Choplin, L. Efficiency enhancement of decontamination gels by a super adsorbent polymer. *Colloids Surf., A* **2014**, *454*, 89−95.
(8) McCafferty, E. *Introduction to Corrosion Science*; Springer: Washington DC, 2006.
(9) Carroll, S. A.; Roberts, S. K.; Criscenti, L. J.; O'Day, P. A. Surface complexation model for strontium sorption to amorphous silica and goethite. *Geochem. Trans.* **2008**, *9*, 2.
(10) Fujii, T.; Yamana, H.; Takamiya, K.; Watanabe, M.; Moriyama, H. Adsorption of fission products on a metal surface in nitric acid solutions: Radiochemical study using a multitracer. *J. Radioanal. Nucl. Chem.* **2002**, *253*, 199−204.
(11) Rouppert, F.; Rivoallan, A.; Largeron, C. An investigation of the chemical equilibria involving cesium, metal oxides and hydroxides on stainless steel. In-situ study of the contaminant sorption modes using fourier transform infrared spectrometry, transport and desorption of radio-contaminants. *Waste Management '00 Conference Proceedings*: Tucson, 2000.
(12) Kádár, P.; Varga, K.; Baja, B.; Németh, Z.; Vajda, N.; Stefánka, Z.; Kövér, L.; Cserny, I.; Tóth, J.; Pintér, T.; Schunk, J. Accumulation of uranium, transuranium and fission products on stainless steel surfaces II. sorption studies in a laboratory model system. *J. Radioanal. Nucl. Chem.* **2011**, *288*, 943−954.
(13) Castle, J. E. The composition of metal surfaces after atmospheric exposure: An historical perspective. *J. Adhes.* **2008**, *84*, 368−388.
(14) Kerry, T.; Banford, A. W.; Thompson, O. R.; Carey, T.; Schild, D.; Geist, A.; Sharrad, C. A. Transuranic contamination of stainless steel in nitric acid. *J. Nucl. Mater.* **2017**, *493*, 436−441.
(15) Bower, W. R.; Morris, K.; Mosselmans, J. F. W.; Thompson, O. R.; Banford, A. W.; Law, K.; Pattrick, R. A. D. Characterising legacy spent nuclear fuel pond materials using microfocus X-ray absorption spectroscopy. *J. Hazard. Mater.* **2016**, *317*, 97−107.
(16) Dombovári, P.; Kádár, P.; Kovács, T.; Somlai, J.; Radó, K.; Varga, I.; Buják, R.; Varga, K.; Halmos, P.; Borszéki, J.; Kónya, J.; Nagy, N. M.; Kövér, L.; Varga, D.; Cserny, I.; Tóth, J.; Fodor, L.; Horváth, A.; Pintér, T.; Schunk, J. Accumulation of uranium on austenitic stainless steel surfaces. *Electrochim. Acta* **2007**, *52*, 2542−2551.
(17) Répánszki, R.; Zsolt, K. Kinetics of fission products accumulation on structural materials. *J. Radioanal. Nucl. Chem.* **2011**, *288*, 729−733.
(18) NDA. *2013 UK Radioactive Waste Inventory: Radioactive Waste Composition*; Moor Row: Cumbria, 2014.
(19) Wallbridge, S.; Banford, A.; Azapagic, A. Life cycle environmental impacts of decommissioning Magnox nuclear power plants in the UK. *Int. J. Life Cycle Assess.* **2013**, *18*, 990−1008.
(20) Demmer, R.; Drake, J.; James, R. Understanding Mechanisms of Radiological Contamination. *WM2014 Conference*: Phoenix, AZ, 2014.
(21) Gui, Y.; Zheng, Z. J.; Gao, Y. The bi-layer structure and the higher compactness of a passive film on nanocrystalline 304 stainless steel. *Thin Solid Films* **2016**, *599*, 64−71.
(22) Mudali, U. K.; Dayal, R. K.; Gnanamoorthy, J. B. Corrosion studies on materials of construction for spent nuclear fuel reprocessing plant equipment. *J. Nucl. Mater.* **1993**, *203*, 73−82.
(23) Robin, R.; Miserque, F.; Spagnol, V. Correlation between composition of passive layer and corrosion behavior of high Si containing austenitic stainless steels in nitric acid. *J. Nucl. Mater.* **2008**, *375*, 65−71.
(24) Priya, R.; Mallika, C.; Mudali, U. K. Corrosion behavior of sensitized 304 SS in nitric acid medium containing oxidizing ions. *Trans. Indian Inst. Met.* **2014**, *67*, 459−467.
(25) Freire, L.; Catarino, M. A.; Godinho, M. I.; Ferreira, M. J.; Ferreira, M. G. S.; Simões, A. M. P.; Montemor, M. F. Electrochemical and analytical investigation of passive films formed on stainless steels in alkaline media. *Cem. Concr. Compos.* **2012**, *34*, 1075−1081.
(26) Liu, J.; Zhang, T.; Meng, G.; Shao, Y.; Wang, F. Effect of pitting nucleation on critical pitting temperature of 316L stainless steel by nitric acid passivation. *Corros. Sci.* **2015**, *91*, 232−244.
(27) Ostolska, I.; Wiśniewska, M. Investigation of the colloidal Cr2O3 removal possibilities from aqueous solution using the ionic polyamino acid block copolymers. *J. Hazard. Mater.* **2015**, *290*, 69−77.
(28) Lang, R. D. L. E.; Engelberg, C.; Walther, M.; Weiss, H.; Bosco, A.; Jenkins, F. R.; Livens, T. W.; Law, G. T. W. Cesium and Strontium Contamination of Nuclear Plant Stainless Steel: Implications for Decommissioning and Waste Minimization. *ACS Omega* **2019**, *4*, 14420−14429.
(29) Kerry, T.; Banford, A. W.; Bower, W.; Thompson, O. R.; Carey, T.; Mosselmans, J. F. W.; Ignatyev, K.; Sharrad, C. A. Uranium Contamination of Stainless Steel in Nuclear Processing Plants. *Ind. Eng. Chem. Res.* **2018**, *57*, 3957−3962.
(30) Gattu, V. K.; Han, S.; Chen, X.; Park, H. S.; Ebert, W. L.; Indacochea, J. E. Impact of added Inconel and stainless steel on zirconium-based alloys for nuclear waste applications. *Corros. Eng., Sci. Technol.* **2022**, *57*, 311−321.
(31) Gattu, V. K.; Ebert, W. L.; Indacochea, J. E.; Frank, S. M. Electrochemical corrosion of a multiphase alloy/oxide composite nuclear waste form. *Corros. Sci.* **2021**, *184*, 109358.
(32) Gattu, V. K.; Ebert, W. L.; Indacochea, J. E.; Cruse, T. A.; Fortner, J. A. Electrochemical corrosion of multiphase stainless steel-based alloy nuclear waste forms. *npj Mater. Degrad.* **2022**, *6*, 14.
(33) Schmuki, P. From Bacon to barriers: a review on the passivity of metals and alloys. *J. Solid State Electrochem.* **2002**, *6*, 145−164.
(34) Huang, Y.; Peng, G.; Chen, B.; Yong, P.; Yao, N.; Yang, L.; Pirraco, R. P.; Reis, R. L.; Chen, J. Preparation and characteristics of the sulfonated chitosan derivatives electrodeposited onto 316l stainless steel surface. *J. Biomater. Sci., Polym. Ed.* **2018**, *29*, 236−256.
(35) Vikneshvaran, S.; Velmathi, V. Schiff Bases of 2,5-Thiophenedicarboxaldehyde as Corrosion Inhibitor for Stainless Steel under Acidic Medium: Experimental, Quantum Chemical and Surface Studies. *ChemistrySelect* **2019**, *4*, 387−392.
(36) Thakur, A.; Kumar, A. Sustainable Inhibitors for Corrosion Mitigation in Aggressive Corrosive Media: A Comprehensive Study. *J. Bio- Tribo-Corros.* **2021**, *7*, 67.

https://doi.org/10.1021/acsomega.2c03535
ACS Omega 2022, 7, 34190−34199